

# $Sr_{14}Cu_{24}O_{41}$ : a complete model for the chain sub-system

Alain Gellé<sup>1</sup> and Marie-Bernadette Lepetit<sup>1,2</sup>

<sup>1</sup> Laboratoire de Physique Quantique, IRSAMC - CNRS UMR 5626, Université Paul Sabatier, 118 route de Narbonne, F-31062 Toulouse Cedex 4, FRANCE

<sup>2</sup> Laboratoire CRISMAT, ENSICAEN - CNRS UMR 6508, 6 boulevard Maréchal Juin, F-14050 Caen Cedex, France  
e-mail: lepetit@ensicaen.fr

December 22, 2018

**Abstract.** A second neighbor  $t-J+V$  model for the chain subsystem of the  $Sr_{14}Cu_{24}O_{41}$  has been extracted from ab-initio calculations. This model does not use periodic approximation but describes the entire chain through the use of the four-dimensional crystallographic description. Second neighbors interactions are found to be of same order than the first neighbors ones. The computed values of the second neighbors magnetic interaction are coherent with experimental estimations of the intra-dimer magnetic interactions, even if slightly smaller. The reasons of this underestimation are detailed. The computed model allowed us to understand the origin of the chain dimerisation and predicts correctly the relative occurrence of dimers and free spins. The orbitals respectively supporting the magnetic electrons and the holes have been found to be essentially supported by the copper  $3d$  orbitals (spins) and the surrounding oxygen  $2p$  orbitals (holes), thus giving a strong footing to the existence of Zhang-Rice singlets.

**PACS.** 7.10.Fd, 71.27.+a, 71.23.Ft

## 1 Introduction

One-dimensional quantum systems have attracted a lot of attention in the past decade due to the large diversity of their low energy physics. In particular, spin-chains and spin-ladders systems have been extensively studied. The characteristic of the  $Sr_{14-x}A_xCu_{24}O_{41}$  ( $A = Ca, Ba, Y, Bi$ , etc.) family of transition-metal oxides is that they are composed of both spin-chains and spin-ladders sub-systems. These compounds are formed of alternated layers (in the  $(a, c)$  plane) of each of the two subsystems [1]. Both ladders and chains are in the  $\mathbf{c}$  direction, however their respective translation vector ( $\mathbf{c}_c$  and  $\mathbf{c}_l$ ) are incommensurate. In the pure compound,  $Sr_{14}Cu_{24}O_{41}$ , the layers are largely separated ( $\simeq 3.3$  Å) and considered as electronically non interacting. Nevertheless, the low energy properties of  $Sr_{14}Cu_{24}O_{41}$  agree neither with those of spin chains, nor with the properties of spin ladders.

$Sr_{14}Cu_{24}O_{41}$  is a semiconductor with a 0.18 eV gap [2] at  $T < T^* = 250$  K. The spin ladders have a singlet ground state with a spin gap of about 35 – 47 meV [3, 4, 5]. Surprisingly the spin chains also exhibit a singlet ground state with a spin gap of 11 – 12 meV [2, 5, 6, 7, 8] while homogeneous spin chains are known to be gap-less in the spin channel. Susceptibility and ESR measurement [9, 2] suggested that the spin gap in the chains is due to the formation of weakly interacting spin dimers. Neutron scattering experiments [3] have later confirmed their existence.

The spins are supported in the chain subsystem by the  $3d_{ac}$  orbitals of the  $Cu^{2+}$  ions, and in the ladder subsystem by the  $3d_{a^2-c^2}$  orbitals of the  $Cu^{2+}$  ions. In the chain subsystem the magnetic orbitals are coupled via two nearly  $90^\circ$   $Cu-O-Cu$  bonds. Let us note at this point that, in such geometries, the super-exchange paths through the oxygen orbitals interact destructively and therefore nearest-neighbor (NN) exchange interactions are expected to be small and ferromagnetic. In the ladder subsystem, the picture of the NN interactions is very different since there are mediated via nearly  $180^\circ$   $Cu-O-Cu$  angles. Such geometries are known to produce strong super-exchange mechanism via the bridging ligands and thus large anti-ferromagnetic interactions.

Formal charge analysis shows that the  $Sr_{14}Cu_{24}O_{41}$  compound is intrinsically doped with six holes by formula unit (f.u.). Similar to high- $T_c$  superconductors, the holes were expected to be mainly supported by the oxygen  $2p$  orbitals and to form Zhang-Rice [10] singlets with the associated-copper hole. NEXAFS (Near Edge X-ray Absorption Fine Structure) experiments [11] later supported this assumption.

It has been established, from neutron scattering [3] and X ray spectroscopy [12] experiments, that the chain dimeric units are formed by two next-nearest-neighbor (NNN) spins separated by a hole.  $Cu$  NMR measurements exhibited the presence of two kinds of holes on the chains [4], namely with intra- and inter-dimer localization. The relative occurrence of the two types of holes ( $0.65 \simeq 1/2$ ) led

the authors to propose a charge-order model with dimers separated by two holes. This assumption has been confirmed by neutron scattering experiments [7, 13] that have shown to be consistent with a five units periodicity. Such a picture leads to a chain filling of 6 holes per f.u., that is with all the holes located on the chains.

The question of the holes repartition between the chain and ladder subsystems is however still under debate. Indeed, NEXAFS experiments [11] evaluated to 0.8 the number of holes on the ladders legs oxygens. Magnetic susceptibility measurements [2] exhibit a filling of 3.5 spins per f.u., that is 0.5 more holes than the maximum number given by the formal charge analysis. Finally, magnon-hole scattering experiments [14] suggest a total localization of the holes on the chain subsystem for temperatures lower than  $T^* \simeq 200$  K.

The origin of the chain electronic dimerisation has only recently being elucidated. The hypothesis of a spin-Peierls transition has been rapidly eliminated since the expected signatures in the magnetic susceptibility and specific heat were not found. It thus has long been supposed that the dimerisation originates from the competition between first and second-neighbor spin interactions as predicted by Majumdar and Gosh [15] and Haldane [16]. We recently showed, using ab initio calculation, that the origin of the dimerized state is of structural origin, even if not of spin-Peierls one [17]. Indeed, this is the structural incommensurate modulations of the chain subsystem, with the periodicity of the ladder one, that strongly modulate the spin/hole orbital energy and localize the spins in a dimer pattern.

These incommensurate structural modulations, that are most of the time neglected, have thus proved to be crucial for the low energy properties of this system. Independently to the on-site orbital energy modulations, the structural distortions of the chain subsystem were shown to be responsible for strong modulation of the first neighbor effective interactions [17], namely NN hopping and NN exchange integrals. One can thus suppose that these structural modulations will also affect the second neighbor interactions that are expected to be of the same order of magnitude than the NN ones in these  $90^\circ$  oxygen bridged systems. Indeed, while the super-exchange path through the bridging oxygens is hindered in the NN interactions, this is not the case for NNN ones where interaction paths through two oxygen bridges are favored. In addition, these second neighbor effective integrals are crucial for the low energy properties of this system since the structural modulations localize the spins into NNN dimers.

The present work thus aims at giving a complete description of the chain subsystem within a second neighbor  $t - J + V$  model, taking explicitly into account the structural incommensurate modulations. The incommensurate character of the problem will be treated within the four-dimensional representation and we will describe the electronic structure without the use of a periodic approximation. Using this complete model, we will further analyze our results as a function of the four crystallographic coordinate and in particular study the different

(quasi)independent spin entities, their relative proportion and positions. This four dimensional method presents the advantage of giving a complete description of these incommensurate systems, without the use of any periodic approximation.

The next section will describe the ab-initio methods used in the present calculations. Section III will analyze the nature of the holes and yield ab-initio evidence of Zhang-Rice singlets. Section IV will give the second neighbor  $t - J + V$  model as a function of the fourth crystallographic coordinate  $\tau$ . Section V will details the NNN double-bridged super-exchange mechanism and its calculations. Section VI will analyze the exchange fluctuations along the chains. Finally the last section will conclude.

## 2 The ab-initio method

It is well known that magnetic and transfer interactions are essentially local in strongly correlated systems and can thus be accurately evaluated using embedded fragment ab-initio spectroscopy methods [18]. The long range electrostatic effects are treated within a bath composed of total-ion pseudo-potentials [19] and charges. The open-shell character of the magnetic/hole orbitals, the strong electronic correlation as well as the screening effects are efficiently treated using quantum-chemistry ab-initio spectroscopy methods. The present calculations were performed using the Difference-Dedicated Configuration Interaction method [20] (DDCI). This configuration interaction method has been specifically developed in order to accurately calculate the low energy states (spectrum and wave functions) of open-shell, strongly correlated formally finite systems. Used on embedded crystal fragments, the DDCI method allow to obtain effective local interactions with a great accuracy and reliability. For instance, it was proved to be very efficient on copper and vanadium compounds such as high  $T_c$  copper oxides [21] or the famous  $\alpha'NaV_2O_5$  compound [22].

The quantum fragments are defined so that to include (i) the magnetic centers, (ii) the bridging oxygens mediating the interactions, and (iii) the first coordination shell of the preceding atoms which is responsible for the essential part of the screening effects. Second-neighbor interactions are thus extracted using three centers  $Cu_3O_8$  fragments (see figure 1b). NNN exchange interactions  $J_2$  are obtained from the doublet-quartet excitations energies when three magnetic electrons are considered. NNN hopping and first neighbor bi-electronic Coulomb repulsion are obtained from the 3 singlets and 3 triplets of the fragment containing one magnetic electron less. Let us point out that the 3 centers calculations also yield the NN interactions, which were previously obtained using two centers  $Cu_2O_6$  fragments [17]. The comparison between the evaluations of the first-neighbor integrals obtained from the 2 centers and 3 centers fragments allows us to verify the relevance of the chosen model and the fragment size dependence of our calculations.

A least-square fit method is used in order to extract the effective parameters from the ab-initio calculations. The

conditions imposed for this purpose are that the effective model should reproduce

- the computed excitation energies,
- the projection of the computed wave-functions within the configuration space generated by the magnetic orbitals.

Let us note that the norm of the later projections give us a measure of the model validity. Indeed, in the present work, the ab-initio wave-functions (which are expanded over several millions of configurations) project over the model configuration space based only on the magnetic orbitals (typically of the order of 10 configurations), with a norm as large as 0.8. One can thus assume that this model space is appropriate to describe the low energy physics of the system.

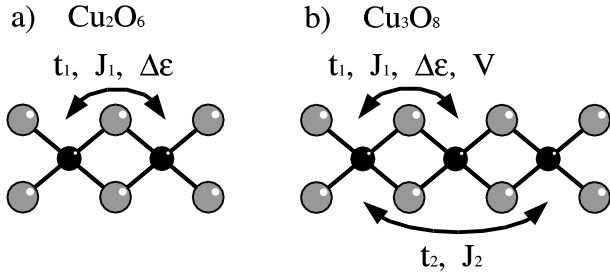


**Fig. 1.** a) Schematic representation of the computed fragments. a) two centers b) three centers. The gray circles represent oxygen atoms, while the black circles represent the copper atoms.

Let us now address the embedding problem for incommensurate systems. The usual embedding technique consists of reproducing the Madelung potential using a set of point charges, located at the crystallographic positions over a box of at least 15 to 20 Å around the fragment [23]. These charges are adjusted on the bath borders according to an Evjen procedure [24]. In the case of a periodic ionic crystal this method insures the nullity of both the system charge and dipole moment. These two conditions are necessary to insure a good representation of the Madelung potential. In the present incommensurate case, however, the Evjen procedure fails to suppress the dipole moment. This is due to the fact that the chain and ladder subsystems are not electrostatically neutral. The relative displacement of one compared to the other thus induces a dipole moment in the chain/ladder direction. In order to solve this problem, and to cancel out the dipole moment contribution, we adjusted the charges of the outermost unit cells of each subsystem, in the  $c$  direction, using a global scaling factor for each adjusted cell [25].

The calculations have been done on 11 equivalent fragments located at 11 successive positions in the chain direction. These 11 fragments give a quite good representation of the different distortions occurring on the chain sub-system. In order to fully represent the whole chain sub-system, these 11 sets of results have been extrapolated,

using Fourier’s series analysis, as a function of the crystallographic fourth coordinate  $\tau$ , which is associated with the system incommensurate modulations.

Let us notice that in a complete crystallographic description [26], each atom possesses a fourth fractional coordinate  $\tau_i = \mathbf{r}_i \cdot \mathbf{k} = z_i c_c / c_l$ , where  $\mathbf{r}_i$  is the atom position in the average structure,  $\mathbf{k} = \mathbf{c}_c^* c_c / c_l$  is the modulation vector,  $z_i$  is the fractional coordinate of the atom in the  $c$  direction. In the model Hamiltonian used in the present work,  $\tau$  corresponds to the fourth coordinate of the chain unit-cell copper atom. It is defined except for a constant.

### 3 Nature of the holes

As previously noticed, it has been supposed in the literature that the holes (both in the chain and ladder subsystems) are not located on the copper atoms but rather on the surrounding oxygens. This assumption has been done by analogy with the high  $T_c$  copper oxides and has later been comforted by NEXAFS experiments [11] as far as ladder holes are concerned. We have thus derived from our ab-initio calculations the nature and composition of both the magnetic (supporting the spins) and hole orbitals.

The magnetic orbitals have been obtained, from the 2 centers fragment calculations, as the triplet natural orbitals (eigenfunctions of the one-electron density matrix) with an occupation number close to 1. In order to locate the hole orbitals we compared two calculations on the same fragment with one electron difference. The hole orbitals have been extracted from the difference between twice the triplet density-matrix and the sum of the two doublet ones. The hole orbitals are thus the two eigenfunctions of the resulting matrix associated with eigenvalues close to 1.

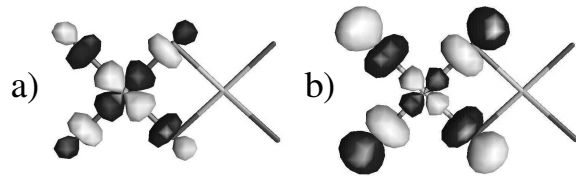


**Fig. 2.** a) Example of magnetic orbital supporting the spin, b) associated hole orbital.

Figure 2 represents a typical example of both the magnetic (a) and hole (b) orbitals on a site. It clearly appears that while the magnetic orbital is essentially supported by the  $3d_{ac}$  copper orbital with a delocalization tail on the surrounding  $2p$  oxygens orbitals, the hole orbital is essentially supported by the  $2p$  oxygen orbitals with a small tail on the  $3d_{ac}$  orbital of the copper atom. The average repartition between copper and oxygens — over the 11 calculations — are as follow :

- for the magnetic orbital : 67% on the copper and 33% on the oxygens,

- for the hole orbital : 15% on the copper and 85% on the oxygens.

The fluctuation of the above repartition on the 11 computed fragments is very small with a standard deviation of only 1.3%. This stability of the copper-oxygen composition of the hole and spin supporting orbitals is quite noticeable since the electrostatic potential modulation on both the copper and oxygen atoms are very strong, with an amplitude of 4eV. Finally, we would like to point out the stronger oxygen character of the hole orbitals in this compound, compared to what was found by Calzado *et al* [27] in the high  $T_c$  parent compound  $La_2CuO_4$ . Indeed, they found only a 50 % oxygen character of the hole supporting orbital.

The present results show the existence of different orbitals, respectively supporting the spins and the holes, and constitute a direct evidence of the ZR singlets in the system.

### 4 Second neighbor $t - J + V$ model

The parameters of a second neighbor  $t - J + V$  model (see eq. 1) were extracted from the ab initio calculations on the eleven positions of the fragments along the chain.

$$\begin{aligned}
 H_{t-J+V} = & \sum_i \varepsilon(\tau_i) n_i \\
 & + \sum_i t_1(\tau_i) \sum_{\sigma} \left( a_{i,\sigma}^{\dagger} a_{i+1,\sigma} + a_{i+1,\sigma}^{\dagger} a_{i,\sigma} \right) \\
 & - \sum_i J_1(\tau_i) (\mathbf{S}_i \mathbf{S}_{i+1} - 1/4 n_i n_{i+1}) \\
 & + \sum_i t_2(\tau_i) \sum_{\sigma} \left( a_{i,\sigma}^{\dagger} a_{i+2,\sigma} + a_{i+2,\sigma}^{\dagger} a_{i,\sigma} \right) \\
 & - \sum_i J_2(\tau_i) (\mathbf{S}_i \mathbf{S}_{i+2} - 1/4 n_i n_{i+2}) \\
 & + \sum_i V(\tau_i) n_i n_{i+1} \tag{1}
 \end{aligned}$$

where  $\tau_i$  is the fourth coordinate of site  $i$ .  $a_{i,\sigma}^{\dagger}$ ,  $a_{i,\sigma}$  and  $n_i$  are the usual creation, annihilation and number operators,  $\sigma$  is the spin quantum number.

We thus obtained eleven sets of parameters that were further fitted as a function of the fourth crystallographic coordinate  $\tau_i$ . The fit was done using Fourier series, according to the following expression

$$a_0 + \sum_n a_n \cos(2\pi n \tau - \varphi_n) \tag{2}$$

Only terms with a non negligible contribution to the series have been retained. It results that the orbital energies, hopping integrals and NN repulsion terms can accurately be obtained from a unique cosine. Exchange integrals, however, necessitate two components to be reliably reproduced, as can be expected from the quadratic dependence of the latter to the hopping integrals.

The results are summarized in table 1. Let us notice that only terms with even frequencies have a non negligible contribution ( $n = 2$  and  $n = 4$  in eq. 2). This can be interpreted as a doubling of the modulation vector  $\mathbf{k}$ . The fourth coordinate of a unit cell is thus given by

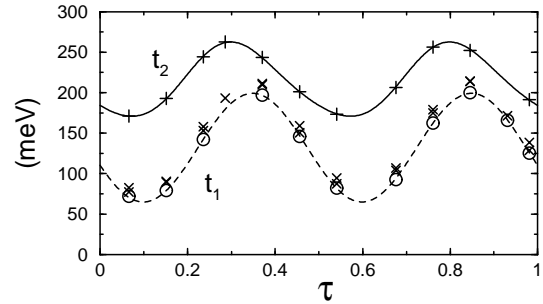
$$\tau = z \times 2 c_c / c_l \simeq z \times 2 \times 7/10$$

where  $z$  is the fractional coordinate in the  $\mathbf{c}$  direction of the unit cell copper atom. It thus clearly appears that the model Hamiltonian presents a 5 unit cells quasi-periodicity. This point is in agreement with the neutron scattering experiments [7,13] that see a pseudo periodicity of the spin arrangement corresponding to five chain unit cells.

meV	$\varepsilon$	$V$	$t_1$	$t_2$	$J_1$	$J_2$
$a_0$	0	661	132.0	214.3	20.88	-6.81
$a_2$	600	-63	-67.2	-45.3	-2.63	1.80
$a_4$				4.2	-2.29	0.26
$\varphi_2$	0	-0.353	-0.401	-0.442	-0.329	-0.450
$\varphi_4$				0.521	-0.411	-0.368

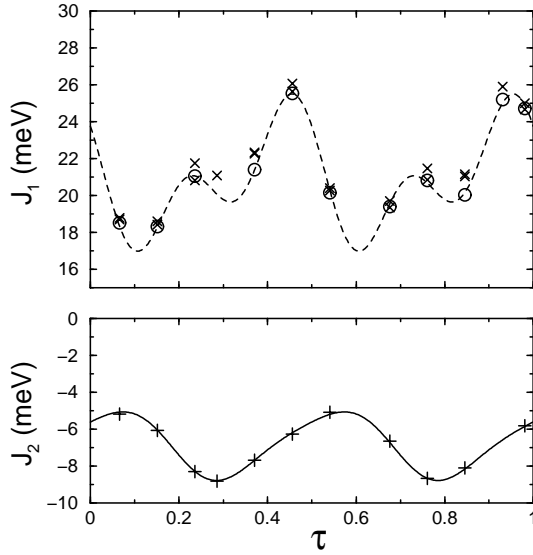
**Table 1.** Analytic fit of the  $t - J + V$  second neighbor model.

Figure 3 reports the effective hopping integrals while figure 4 reports the effective exchange integrals. Both are given as a function of the fourth crystallographic coordinate  $\tau$  (defined as in the Hamiltonian expression).



**Fig. 3.** NN and NNN effective hopping integrals as a function of  $\tau$ . The circles correspond to the two-coppers fragment calculations, the cross to the three-coppers calculations and the lines to the Fourier fits.

The NN integrals have been evaluated both from the two-centers and three-centers fragments. The three-centers fragments used in the calculations have been chosen in successive positions along the chain, thus, each NN integral appears in two successive fragments yielding independent evaluations. One should first notice that the three independent evaluations of the the NN hopping,  $t_1$ , and exchange,  $J_1$ , integrals yield the same values, thus validating (i) the second neighbor  $t - J + V$  model used in the present work and (ii) the strong locality of the interactions. Indeed, whether other interactions or orbitals would have been of importance, whether the integrals screening



**Fig. 4.** NN and NNN effective exchange integrals as a function of  $\tau$ . The circles correspond to the two-coppers fragment calculations, the cross to the three-coppers calculations and the lines to the Fourier fits.

effects would have a larger range than the first coordination shell of the magnetic atoms, the two-centers and three-centers calculations would have given different evaluations of the integrals so that to compensate the inability for the model to reproduce the low-energy local physics.

As expected, the NNN interactions are of the same order of magnitude as the NN ones. In fact, the second neighbor hopping integrals are even nearly twice as large in amplitude as the first neighbor ones. Indeed, while the NN hole orbitals are nearly orthogonal, the NNN hole orbitals strongly overlap (see figure 2b). Another important point is the strong modulation of the hopping integrals as a function of  $\tau$ . The  $t_2$  modulation amplitude is 88 meV and represents a 15% standart deviation around an average amplitude of 214meV.

NN and NNN exchange integrals are, as expected, different in nature with ferromagnetic NN exchange and antiferromagnetic NNN one. This is due to the usual well known reasons (i) the direct exchange integral, which is always ferromagnetic in nature, decreases exponentially with the  $Cu-Cu$  distance and thus becomes negligible between NNN centers, (ii) the super-exchange term, mediated via the bridging oxygen  $2p$  orbitals and antiferromagnetic, is hindered in the NN case due to the destructive interaction of the bridging orbitals. It results for the NNN exchange a weak, antiferromagnetic integral, in agreement with the experimental findings [2]. Two points are however worth noticing.

- The experimental evaluation of the intra-dimer exchange  $J_d$  is  $-11$  meV, that is somewhat larger than our findings for NNN exchange.
- The computed  $J_2$  integral strongly vary along the chain since its amplitude variation is 55 % of its mean value

$-7$  meV. This strong modulation is however not observed in neutron scattering experiments [13].

These two important points are discussed in the following sections.

## 5 Super-exchange mechanism through a double bridge

The DDCI method used in this work is well known to give reliable and very accurate evaluation of the NN exchange integrals. It has been used with a lot of success for computing NN exchange integrals in copper [21,27], nickel [28], vanadium [22] and other oxides. Indeed, it was shown that in order to accurately compute magnetic integrals, the following effects should be treated [29,30,31,32] :

- the multideterminantal and open-shell character of the reference wave function,
- the correlation within the magnetic orbital shell,
- the screening effects (dynamical polarization) on the different configurations of the reference wave function,
- the effect of the ligand to metal charge transfers configurations that mediate the interaction,
- and the screening effects on the latter configurations.

The characteristic of the DDCI method is to treat all these effects in the case of interactions mediated by at most one bridging entity.

In the present case, the NNN interactions are mediated by **two** and not one bridging entities, namely the two oxygens between the first and second copper and the two oxygens between the second and third copper. It results a perturbative evaluation of the  $J_2$  integral within a two bands (magnetic plus bridging entities) extended Hubbard model of

$$J_2 = -4 \frac{t_{pd}^4 t_{pp}^2}{\Delta_1^4 U_d} - 4 \frac{t_{pd}^4 t_{pp}^2}{\Delta_1^4 \Delta_2'} - 16 \frac{t_{pd}^4 t_{pp}^2}{\Delta_1^3 \Delta_2 \Delta_2'} - 16 \frac{t_{pd}^4 t_{pp}^2}{\Delta_1^2 \Delta_2^2 \Delta_2'}$$

where  $t_{pd}$  is the hopping integral between the copper magnetic orbital and the bridging oxygen  $2p$  orbitals and  $t_{pp}$  is the hopping between the orbitals of the two bridging entities.  $\Delta_1$  is the excitation energy between the reference configurations and the single ligand-to-metal charge transfer configurations.  $\Delta_2$  and  $\Delta_2'$  are the excitation energies of the double charge transfers configurations,  $\Delta_2$  when the holes are on different bridging entities and  $\Delta_2'$  when they are on the same. Figure 5 pictures the different perturbative mechanisms yielding the above equation. One sees that out of the twenty possible paths, only two of them do not involve double ligand-to-metal charge transfer configurations. Thus, even-though the double charge transfer excitations are of higher energy than the single ones (of the order of twice as large), they are much more numerous and thus should be responsible for a large part of the  $J_2$  effective integral, unlike the case of single bridged integrals. One should now remember that while the DDCI method

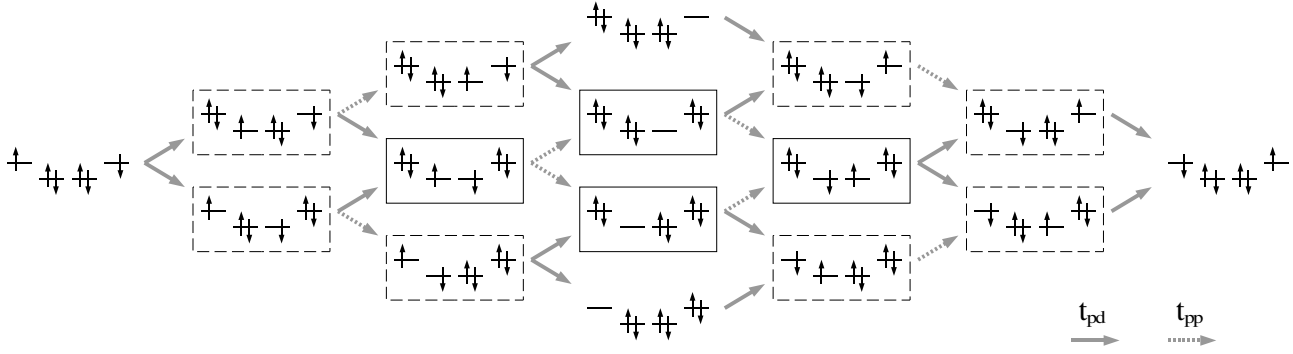


**Fig. 5.** Perturbative mechanism of the NNN effective exchange integrals mediated through two bridging entities. In each configuration, the relative position of the orbitals are pictured in energy scale, that is the two higher orbitals are the magnetic copper ones and the two lower orbitals are the  $2p$  bridging entities orbitals. The single ligand-to metal charge transfer configurations are frame with dashed lines and the double transfer ts with solid lines. The copper to ligand  $t_{pd}$  hopping integrals are pictured with solid arrows while the ligand to ligand hoppings,  $t_{pp}$ , are with dashed arrows.

correctly compute the screening effect of the ligand-to-metal charge transfer configurations, this is not the case for the double charge transfer ones [30]. It results that the excitation energies toward the double charge transfer configurations ( $\Delta_2$  and  $\Delta'_2$ ) are overestimated and the that thus the  $J_2$  integral is underestimated in the present calculation. Unfortunately including the screening effects of the double charge transfers is technically not possible at this time since it would involve triply excited configurations compared to the reference ones.

It is important to point out that a similar perturbative analysis of the NN integrals as well as the NNN hopping integral shows that the contribution of the double charge transfers are negligible in these cases. Moreover, noticing that the  $J_2$  modulations are essentially due do the modulations of the transfer integrals ( $t_{pd}$  and  $t_{pp}$ ), the relative variations of  $J_2$  can be assumed to be correctly reproduced in the present calculations.

### 6 Second neighbor exchange fluctuations along the chains

Let us now address the question of the NNN exchange fluctuations along the chain. As previously mentioned the neutron scattering experiments do not see much fluctuations of the intradimer effective exchange. In order to compare our results with the experimental ones one should determine which among all the NNN exchange integrals along the chain correspond to an intradimer spin coupling.

In incommensurate systems, the real space analyses present the drawback to never provide a complete description of the total system. We thus chose to identify the dimer localization along the chain not in the real space but as a function of the fourth crystallographic coordinate  $\tau$ . Even if such an analysis is not as intuitive, it presents the advantage to provide a complete description of the system.

We will thus analyze the system in order to derive a partition into physically pertinents blocks and to determine (i) the number of different type of blocks, (ii) their

relative arrangement and (iii) their rate of existence in the incommensurate structure. For this purpose it is useful to start with a chosen type of block, expected to be largely represented in the system. In the present case we chose the dimeric units. Then, the model Hamiltonian is used to determine the apparition of this type of blocks as a function of the fourth component. The analysis of the remaining sites allows to determine the other types of significant blocks present in the system. Finally, the relative arrangement of the types of blocks can be studied.

The dimeric units are composed of five sites, the three sites of the dimer plus the two ZR singlets of the neighboring sites (see figure 6). Let us use the fourth coordinate

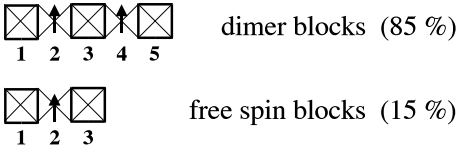


**Fig. 6.** The different types of spin blocks appearing in the chains. Values in parentheses refer to the percentage of the chain corresponding to the different types of blocks.

of the first site ( $\tau_1$ ) as the block reference. If one plots the energy of five consecutive sites as a function of  $\tau_1$ , a dimeric unit will thus be obtained when the energy of the second and fourth sites are below the Fermi level, while the energy of the first, third and fifth sites are above the Fermi level. Figure 7 shows the orbital energy curves of five consecutive sites as a function of  $\tau_1$ . Let us notice that, since five sites are represented by a unique value of  $\tau$ , only one fifth of the  $[0, 1]$  range is necessary to represent the whole chain. The values of  $\tau_1$  for which the five consecutive sites form a dimer are represented in gray. They span two ranges of width 0.085. The proportion of the chain occupied by dimers thus corresponds to five time the above ranges, that is 85% of the whole chain. The number of dimers can then be evaluated to 1.70 per f.u., to be compared to 1.47 dimer per f.u. deduced from mag-

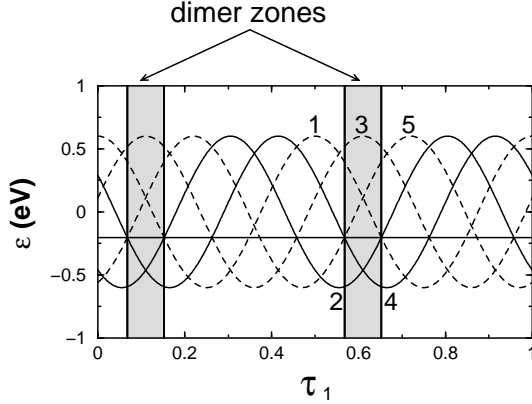


**Fig. 7.** Orbital energy of five consecutive sites as a function of the fourth coordinate  $\tau_1$  of the first one. The horizontal line represent the Fermi level.

netic susceptibility measurements [2]. Let us now analyze the composition of the remaining 15% of the chain. For this purpose we will determine the number of sites separating two consecutive dimers. If  $\tau_1$  is referencing the first dimer (that is  $\tau_1 \in [0.068; 0.153] \cup [0.568; 0.653]$ ) then the reference of the second dimer is given by  $\tau'_1 = \tau_1 + n(\tau_1)c_c/c_l$ , where  $n(\tau_1)$  is the smaller integer such that  $\tau'_1 \in [0.068; 0.153] \cup [0.568; 0.653]$ . At this stage three cases can occur.

1. case.  $n(\tau_1) < 5$ . In this case, the two successive dimers overlap, in other words there exist physical entities larger than the dimers.
2. case.  $n(\tau_1) = 5$ . In this case, the two dimers are strictly consecutive along the chain.
3. case.  $n(\tau_1) > 5$ . In this case, the two successive dimers are separated by one or several other type of blocks of total length :  $n(\tau_1) - 5$ .

In the present system, only  $n = 5$  and  $n = 8$  occurs. As stated above the former corresponds to consecutive dimers and the latter to dimers separated by three sites blocks. As for the dimers, we will reference these blocks by the fourth coordinate of their first site, that is  $\tau_1 + 5c_c/c_l$ . The three sites blocks thus span two ranges :  $[0.042; 0.068]$  and  $[0.542; 0.568]$ . Figure 8 represents the three sites blocks and the dimer ranges for  $\tau_1 < 0.5$ . In each region, the orbital energy of each site of the block has been represented. One sees immediately that the three sites blocks are formed by one spin surrounded by two ZR singlets. Such a configuration can be associated with free spins since the nearest neighbor spin is two ZR singlets afar. Let us notice that three times the free spins ranges yields 0.15, that is the total missing part of the chain. The number of free spins can be now easily evaluated to 0.5 per f.u., to be compared to 0.55 free spins per f.u. obtained from the magnetic susceptibility experiments.

A further analysis of the figure 7 shows that the dimers are arranged in clusters of three or four dimers separated by a free spin. It can be evaluated that 54% of the dimers form three-dimers clusters while 46% form four-dimers clusters.

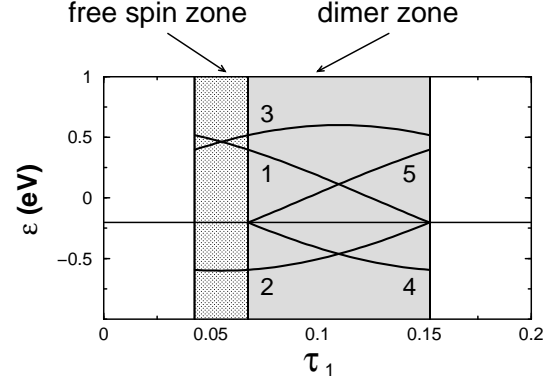


**Fig. 8.** Orbital energy of block sites for the two different types of block given as a function of the fourth coordinate  $\tau_1$  of the first site of each block. The horizontal line represent the Fermi level.

Let us now go back to the intradimer integrals. The regions of  $\tau$  corresponding to dimers are reported in gray on figure 9. The intradimer  $J_2$  regions correspond to  $J_2$

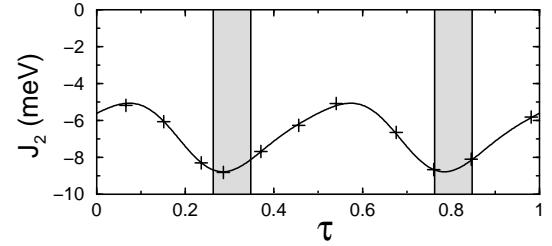


**Fig. 9.** NNN effective exchange integrals as a function of  $\tau$ . The regions in gray correspond to intradimer effective exchange integrals. Let us note that the  $\tau$  values in the present figure is associated with the  $\tau_2$  value of the second site of the 5 centers dimeric units. This results in a shift in the  $\tau$  values compared to figure 7.

values between  $-8.1$  and  $-8.8$  meV.

Our calculations thus yield values of the intradimer exchange that are quite homogeneous since their fluctuation range is smaller than 0.7 meV, that is less than 8% of their nominal values, in good agreement with the neutron scattering experiment (the variation range is within the experimental error bars). The other interesting point is that the  $J_2$  values corresponding to intradimer exchanges are the largest ones in absolute values. The underestimation due to our method is thus quite limited since our average value is  $-8.5$  meV to be compared to the experimental values ranging from 11 and 12 meV.

## 7 Conclusion

To summarize the present results, we have determined a second neighbor  $t - J + V$  model for the incommensurate chain subsystem of the  $Sr_{14}Cu_{24}O_{41}$  compound. The

model parameters have been determined using accurate ab initio calculations on a series of embedded clusters along the chain. In order to obtain a complete model as a function of the incommensurate modulations, the ab initio results have been extrapolated using a Fourier analysis. The resulting model is thus independent of any periodic approximation and is given as a continuous function of the fourth crystallographic coordinate  $\tau$ , which describes the incommensurate modulations along the chain.

It is noticeable that, unlike what is currently assumed in the literature, the various parameters of the model, except for the first neighbor bi-electronic repulsion, strongly vary as a function of the structural incommensurate modulations. In fact, these variations are so large that they determine the physics of the system. In particular, the orbital energies vary over a surprisingly large range, and thus dominate the low energy physics through a strong localization of the electron (resp. holes) over the low (resp. high) energy sites.

The analysis of the model as a function of the fourth crystallographic coordinate  $\tau$  allowed us to show that at low temperature the chain ground state can be entirely described only by second-neighbor dimers and free spins if no hole transfer to the ladder is assumed. It is worth to point out that our estimation of the free spin number per formula unit, 0.5, is under these filling hypothesis in very close agreement with the experimental value of 0.55. Further analysis of our results showed that the dimers are arranged in clusters of three or four units separated by a free spin. The intradimer exchanges are found to be antiferromagnetic, weakly dependent of the dimer position along the chain and in reasonable agreement with the experimental values, even if a little underestimated. It is amazing to realize that while the strong modulation of the model parameters are responsible of the low energy properties of this system and in particular of the electron / hole localization and the resulting formation of the dimers, the parameters range actually seen in magnetic experiments corresponds to a nearly homogeneous dimer system.

Wave functions analysis exhibited holes localization not on the copper atoms but rather on the surrounding oxygen  $2p$  orbitals, thus confirming the hypothesis of the presence of Zhang-Rice singlets. Three types of Zhang-Rice singlets can be identified in our calculations, namely the intra-dimer ones, and two types of inter-dimer ones : those neighboring dimers and those neighboring free spins. This result is to be put in perspective with the copper NMR experiments [4] that sees a splitting of the inter-dimer Zhang-Rice singlets signal at low temperatures. It would be interesting to quantify the relative weight of the two signals in order to check our predicted ratio of 3.4.

**Acknowledgment** : the authors thank Dr. J. Etrillard for providing us with the neutron crystallographic structures as well as for helpful discussions, Dr. D. Maynau for providing us with the CASDI suite of programs, Dr. P. Sciau for introducing us with the four-dimensional crystallographic conventions. The present calculations were

done using the IDRIS computational center facilities under project number 1104.

## References

1. M. McCarron et al., Mater Res. Bull. **23**, 1355 (1988)
2. S.A. Carter *et al.*, Phys. Rev. Lett. **77**, 1378 (1996).
3. R.S. Eccleston, M. Azuma and M. Takano, Phys. Rev. **B 53**, 14721 (1996) ; M. Matsuda *et al.*, Phys. Rev. **B 54**, 12199 (1996).
4. K. Magishi *et al.*, Phys. Rev. **B 57**, 11533 (1998).
5. S. Tsuji *et al.*, J. Phys. Soc. Jap. **65**, 3474 (1996) ; K. Kumagai *et al.*, Phys. Rev. Lett. **78**, 1992 (1997).
6. M. Takigawa *et al.*, Phys. Rev. **B 57**, 1124 (1998).
7. R.S. Eccleston *et al.*, Phys. Rev. Lett. **81**, 1702 (1998).
8. U. Ammerahl *et al.*, Phys. Rev. **B 62**, 8630 (2000).
9. M. Kato, K. Shiota and Y. Koike, Physica C **258**, 284 (1996).
10. F. C. Zhang and T. M. Rice, Phys. Rev. **B 37**, 3759 (1988).
11. N. Nücker *et al.*, Phys. Rev. **B 62**, 14384 (2000).
12. D.E. Cox, I. Iglesias, K. Hirota, G. Shirane, M. Matsuda, N. Motoyama, H. Eisaki and S. Uchida, Phys. Rev. **B 57**, 10750 (1998).
13. L.P. Regnault *et al.*, Phys. Rev. **B 59**, 1055 (1999) ; M. Matsuda *et al.*, Phys. Rev. **B 59**, 1060 (1999).
14. C. Hess, H. El Haes, B. Büchner, U. Ammerahl, M. Hücker and A. Revchikov, Phys. Rev. Letters **93**, 27005 (2004).
15. C. K. Majumdar and D. K. Ghosh, J. Math. Phys **10** 1399 (1969).
16. F. D. M. Haldane, Phys. Rev. **B 25** 4925 (1982).
17. A. Gellé and M.-B. Lepetit, Phys. Rev. Letters **92**, 236402 (2004).
18. M.-B. Lepetit, *Recent Research Developments in Quantum Chemistry*, p. 143, Vol. 3, Transworld research Network (2002) (or cond-mat/0502268).
19. N. W. Winter, R. M. Pitzer and D. K. Temple, *J. Chem. Phys.* **86**, 3549 (1987).
20. J. Miralles, J. P. Daudey and R. Caballol, Chem. Phys. Lett. **198**, 555 (1992) ; V. M. García *et al.*, Chem. Phys. Lett. **238**, 222 (1995) ; V. M. García, M. Reguero and R. Caballol, Theor. Chem. Acc. **98**, 50 (1997).
21. D. Muñoz, F. Illas and I. de P.R. Moreira, Phys. Rev. Letters **84**, 1579 (2000) ; D. Muñoz, I. de P.R. Moreira and F. Illas, Phys. Rev. **B 65**, 224521 (2002).
22. N. Suaud and M.-B. Lepetit, Phys. Rev. **B 62** 402 (2000) ; N. Suaud and M.-B. Lepetit, Phys. Rev. Letters **88**, 056405 (2002).
23. M. Isobe *et al.*, Phys. Rev. **B 62**, 11667 (2000) ; J. Etrillard *et al.*, Physica C, in press.
24. H. M. Evjen, **Phys. Rev.** **39**, 675 (1932).
25. A. Gellé and M.-B. Lepetit, unpublished.
26. P.M. de Wolff, Acta Cryst. A **30**, 777 (1974).
27. C. J. Calzadua, J. F. Sanz and J. P. Malrieu, J. Chem. Phys. **112**, 5158 (2000).
28. I. De P. R. Moreira and F. Illas, Phys. Rev. **B 55**, 4129 (1997) ; C. de Graaf, F. Illas, R. Broer, and W.C. Nieuwpoort, J. Chem. Phys. **106**, 3287 (1997).
29. P. de Loth, P. Cassoux, J. P. Daudey et J. P. Malrieu, J. Am. Chem. Soc., **103**, 4007 (1981).



30. A. Gellé, M. L. Munzarová, MB Lepetit and F. Illas, Phys. Rev. **B 68**, 125103 (2003).
31. C. J. Calzado, J. F. Sanz and J.P. Malrieu, J. Chem. Phys. **112**, 5158 (2002).
32. MB Lepetit, *Recent Research Developments in Quantum Chemistry 3*, p. 143, Transword Research Network (2002).